Nuclear Inst. and Methods in Physics Research B 453 (2019) 67–74

Contents lists available at ScienceDirect

Nuclear Inst. and Methods in Physics Research B

journal homepage: www.elsevier.com/locate/nimb

Influence of tungsten fuzz on energy spectra of helium recoiled by 10 MeV oxygen ions

M. Mayer[a,*], S. Lederer[a,b]

[a] Max-Planck-Institut für Plasmaphysik, Boltzmannstr. 2, 85748 Garching, Germany
[b] Technische Universität München, Fakultät für Physik, James-Franck-Str. 1, 85748 Garching, Germany

ARTICLE INFO

Keywords:
Ion beam analysis
Elastic recoil detection analysis
ERDA
Tungsten fuzz
Surface roughness
Computer simulation

ABSTRACT

The influence of fuzz-like tungsten surface structures on the shape of helium energy spectra recoiled by an incident 10 MeV ^{16}O beam was investigated by computer simulations using the program STRUCTNRA and a phenomenological two-dimensional tungsten fuzz model. The model describes fuzz by a random distribution of inclined rectangular filaments containing tungsten and 1 at% helium. The mean width of the filaments was varied from 10 to 100 nm and the mean filament height was varied from 10 to 1500 nm while keeping the total amount of material constant. The shapes of the helium recoil energy spectra are modified by the fuzz, the deviations from the spectrum of a smooth sample increase with increasing filament widths and heights. The total numbers of detected helium recoils remain surprisingly independent of the filament widths and heights. A surrogate smooth sample with depth profile yielding a recoil energy spectrum identical to a fuzzy sample can be always found. The total amount of He can be derived robustly using the surrogate sample.

1. Introduction

Tungsten is foreseen as armor material for divertor plasma facing components in the ITER fusion experiment due to its very high melting point, high thermal conductivity, high threshold energy for physical sputtering and corresponding low sputtering yields, and low tritium retention. Helium is created as product of D–T fusion reactions during the nuclear deuterium–tritium (DT) operational phase of ITER, but already during the helium operational phase, which is currently foreseen after the protium (HH) and before the deuterium (DD) and deuterium–tritium (DT) operational phases, the divertor will be subject to high fluxes of incident helium ions with energies from a few eV to a few ten eV. Divertor surface temperatures can be above 1000 K. Under these conditions the formation of highly irregular surface structures has been observed, which can consist of pits, holes, bubbles or grass-like structures on the nano- or microscale [1–13]. These surface structures are usually called *tungsten fuzz* [5].

Fuzz is very undesirable in fusion devices as it degrades tungsten properties by reducing its thermal conductivity and yielding a potential source of high-Z dust impurities. Several models for the mechanisms of tungsten fuzz growth have been proposed [4,14–17], but currently there exists no general theoretical agreement on the growth mechanisms.

One key property of tungsten fuzz is its helium content. The experimental determination of the helium concentration in tungsten fuzz is challenging due to the extremely rough surface structures. Gasparyan et al. used thermal desorption spectroscopy (TDS) for determining the total amount of retained helium [11]. TDS requires very high temperatures above 2000 K, is destructive, and provides only information about the total amount of helium retained in the sample but does not provide information about the helium concentration in the fuzz or its distribution with depth. Woller et al. used elastic recoil detection analysis (ERDA) for dynamic measurements of the helium concentration in growing tungsten fuzz using incident oxygen ions [8,9]. Doerner et al. added ^3He to the incident helium plasma and used nuclear reaction analysis (NRA) employing the $^3He(D,p)$ reaction for quantitative measurements of the retained ^3He concentration [18,13].

It is well known that ion beam analysis (IBA) methods like ERDA and NRA are quantitative methods for depth profiling of elements—at least for smooth samples. However, surface roughness can be especially a problem for ERDA, where it has been shown that already moderate surface roughnesses can modify the shape of spectra significantly [19–21]. Simulation methods allowing to quantify IBA measurements on samples with moderate roughness have been developed [22]. However, for samples with such extreme roughnesses like tungsten fuzz it remains unclear how accurately IBA measurements of these samples can be quantified.

In this work we investigate the influence of tungsten fuzz on the

* Corresponding author.
E-mail address: matej.mayer@ipp.mpg.de (M. Mayer).

https://doi.org/10.1016/j.nimb.2019.04.081
Received 4 September 2018; Received in revised form 24 April 2019; Accepted 24 April 2019
Available online 06 June 2019
0168-583X/

shape of ERDA energy spectra by computer simulations using a simplified two-dimensional fuzz model.

2. Computer simulations

2.1. Phenomenological tungsten fuzz model

Scanning or transmission electron micrographs (SEM or TEM) of tungsten fuzz revealed a highly complex structure. The fuzz often consists of individual filaments with irregular shapes and substructures like arches, drops, bends or junctions (see for example [[7] Fig. 1]). The details of this microstructure depend on exposure temperature, incident helium flux and fluence. An accurate description of this microstructure is hardly possible and would require knowledge of the corresponding probability distribution functions (for example of filament width or height), which are not available in the literature.

We therefore use a simplified two-dimensional phenomenological model of tungsten fuzz which reflects the basic microstructure of fuzz. It allows easy and fast creation of fuzzy surface structures and can be used for further simulations. Each filament of the fuzz is approximated by a rectangle. Heights H and widths W of the rectangles are randomly distributed following Γ-distributions with mean value and standard deviation. The starting points of the filaments are randomly distributed in horizontal direction following a uniform distribution with periodic boundary conditions. Each filament is randomly inclined with respect to the surface normal, the inclination angle follows a cosine distribution. Filaments are allowed to intersect. Pixels are assumed to be quadratic with a pixel size of $5 \times 5\ nm^2$, each pixel corresponds to 1.58×10^{10} atoms/cm (see Section 2.2).[1] The image size was always 20480 nm (4096 px) in horizontal direction and between 500 and 4500 nm in vertical direction depending on the heights of the filaments. For short filaments with heights $\leqslant$ 100 nm an additional pedestal, i.e. a smooth rectangle of material was added in order to obtain an identical number of black pixels as in the case of a smooth sample. See Table 1 for the mean values of H and W, their standard deviations, the heights B of the pedestal and the number N of fuzz filaments for all cases.

An additional lower bulk block with a thickness of 75 nm could be added. Examples of simulated tungsten fuzz including the lower block are shown in Figs. 1 and 2. In order to study statistical fluctuations between 5 and 30 different images were created for each combination of mean filament width and height.

The smooth sample had a size of $195 \times 20480\ nm^2$ ($39 \times 4096 = 159744$ black pixels) without lower bulk block and $270 \times 20480\ nm^2$ ($54 \times 4096 = 221184$ black pixels) with lower bulk block. The number of black pixels (black pixel count, BPC) in each generated fuzz image is randomly distributed due to the random distribution of filament heights, widths and intersections between filaments. Because the BPC is proportional to the total amount of material (i.e. the total number of atoms/cm) in the sample, fluctuations of the BPC would result in fluctuations of the simulated ERDA spectra due to fluctuations of the number of atoms/cm. In order to obtain images with identical BPC's only images with a deviation of the BPC below 1% from the smooth sample were used for further simulations[2]. For small filament heights the BPC fluctuations were typically below 0.5%. In the cases with 75 nm thick lower block the fluctuations were smaller due to the additional constant amount of material and fluctuations of the BPC were generally below 0.6% and mostly below 0.3% for small filament heights.

2.2. Simulation of ERDA spectra

ERDA spectra from the generated tungsten fuzz images, see Section 2.1, were simulated using the program STRUCTNRA 2.9 [23,24] using SIMNRA 7.02 [25] as simulation kernel. The composition of black pixels was assumed to be 99 at% W and 1 at% He with a mass density of g/cm^3, white pixels were assumed to be void. The simulated experimental setup used an incident beam of 10 MeV ^{16}O ions at an incident angle of 75° to the surface normal, a recoil angle of 30° and an exit angle of 75°. The recoil cross-sections for ^{3}He and ^{4}He were assumed to be Rutherford, forward scattered ^{16}O ions were not calculated for the sake of minimizing computing time. A stopper foil was not employed, i.e., the calculated recoil spectra are at the sample surface. An infinitesimally small detector (without geometrical energy spread) with an energy resolution of 15 keV was assumed. SRIM 2013 stopping powers were used [26], and the multiple-scattering option of SIMNRA was switched on.

Each pixel of the tungsten fuzz images was split into 3×3 sub-pixels in STRUCTNRA for avoiding oscillations in the simulated spectra, only for very large images the number of sub-pixels was set to 2×2 for reducing computing time. The computing time also increases linearly with the number of incident trajectories: The number of incident trajectories therefore should be kept as small as necessary. In order to determine the necessary number of incident trajectories two images with mean filament width 25 nm, mean filament height 500 nm and with mean filament width 100 nm, mean filament height 500 nm were simulated with 25, 50, 80, 100, 200, 300, 400, 500, 600, 900 and 1200 incident trajectories. Already the spectra simulated with 200 trajectories were very close to the most accurate simulation with 1200 trajectories. Therefore 300 incident trajectories were used for all single images in order to get a reasonable compromise between accuracy and computing time. Between 5 and 30 different images were selected for simulation of the ERDA spectrum for each combination of mean filament width and height, all of which had identical BPC (see Section 2.1).

STRUCTNRA 2.9 is optimized for parallel processing and uses multiple SIMNRA threads. The simulations in this work were performed using typically 32 SIMNRA threads in parallel.

3. Results

Simulated He recoil spectra for 10 MeV incident ^{16}O ions from three different images created from the same set of parameters (mean filament width 25 nm, mean filament height 500 nm, no lower block) are shown in Fig. 3 left. A typical example for simulated fuzz with these parameters (but with lower block) is shown in Fig. 1 middle. Despite the large image width of more than 20 μm spectra from different images show some variation, both with respect to the shape of the spectra and to the total integrated number of recoil counts. The average spectrum from 10 different images (solid black line in Fig. 3 left), corresponding to an image width of more than 200 μm and 3000 incident trajectories, is smooth and shows only very little variation when additional images are added.

A more extreme example of the variability of spectra is shown in Fig. 3 right for a mean filament width of 100 nm and a mean filament height of 1500 nm without lower block, a typical example for simulated fuzz with these parameters (but with lower block) is shown in Fig. 2 bottom. The smaller number of fuzz filaments results in larger fluctuations of spectra from different images, and spectra from about 20 images had to be averaged in order to obtain a stable average spectrum.

Simulated He recoil spectra for 10 MeV incident ^{16}O ions are shown in Fig. 4 for mean filament widths from 25 to 100 nm and mean filaments heights up to 1500 nm, without lower block. Between 6 and 29 spectra from individual images were averaged in order to obtain sufficiently smooth spectra without too large fluctuations. Incident energy and material thickness were selected such that all recoiled He ions reach the detector, i.e., there are no particles lost by getting stuck in the

[1] Note that the unit atoms/cm^2 corresponds to a *length*, while atoms/cm corresponds to an *area*.

[2] Except for very large widths and heights, where scarce deviations up to 3% could not be avoided in some cases.

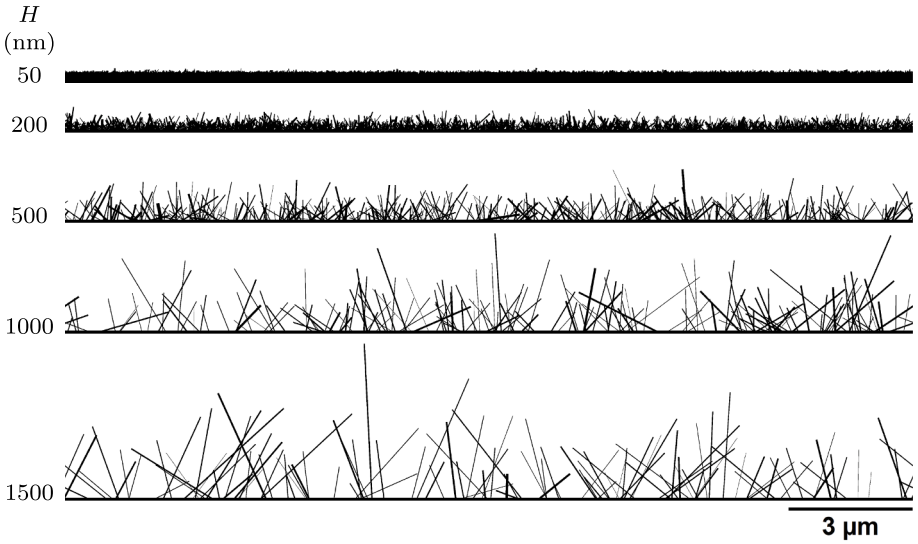

Fig. 1. Typical simulated fuzz images with additional 75 nm lower block for different mean filament heights *H*. Image width 20480 nm, mean filament width 25 nm. See Table 1 for all fuzz parameters.

Table 1
Bulk height *B* (in nm) and number of fuzz filaments *N* for different filament widths *W* and filament heights *H*. *W* and *H* were Γ-distributed with mean value and standard deviation (both in nm) given in the table. See Figs. 1 and 2 for typical fuzz images.

H	*W*							
	10 ± 5		25 ± 10		50 ± 15		100 ± 25	
	B	*N*	*B*	*N*	*B*	*N*	*B*	*N*
Smooth	195	0	195	0	195	0	195	0
10 ± 5	190	4000	180	9000	170	7000	150	7000
25 ± 10	170	9000	160	8500	155	7200	140	5300
50 ± 20	145	7500	125	7500	115	7100	105	5300
75 ± 30	120	7000	90	7500	75	7100	65	4800
100 ± 40	100	6000	50	7500	35	6600	30	3800
200 ± 80	25	4500	0	1800	0	900	0	430
300 ± 120	0	2800	0	880	0	420	0	210
500 ± 200	0	1400	0	430	0	205	0	100
1000 ± 400	0	620	0	195	0	90	0	45
1500 ± 600	0	400	0	125	0	60	0	29

sample structure. With increasing mean filament widths and/or heights the low-energy edge of the He recoil spectra at about 2500 keV gets wider: This is caused by a widening of the distribution of path lengths inside the material. The high energy edge of the He recoil spectra at around 4800 keV bevels with increasing mean filament widths and/or heights. Additionally a small peak develops close to the surface at about 4600 keV: This is due to He ions recoiling through one filament. The energy spectrum from about 3500 keV to about 4500 keV shows only very small changes for the investigated range of filament widths and heights and is almost identical to the spectrum from a smooth sample (solid black line in Fig. 4).

Due to the stochastic nature of the created images the BPC and consequently the total amount of He (measured in atoms/cm) in the simulated samples varies from image to image even for identical input parameters for mean filament width and height. In order to avoid fluctuations due to varying BPC only images with identical BPC, see Section 2.1, were selected for simulations. But even for identical BPC and hence identical amounts of He atoms/cm in the sample the calculated number of He recoils fluctuates from image to image. This is due

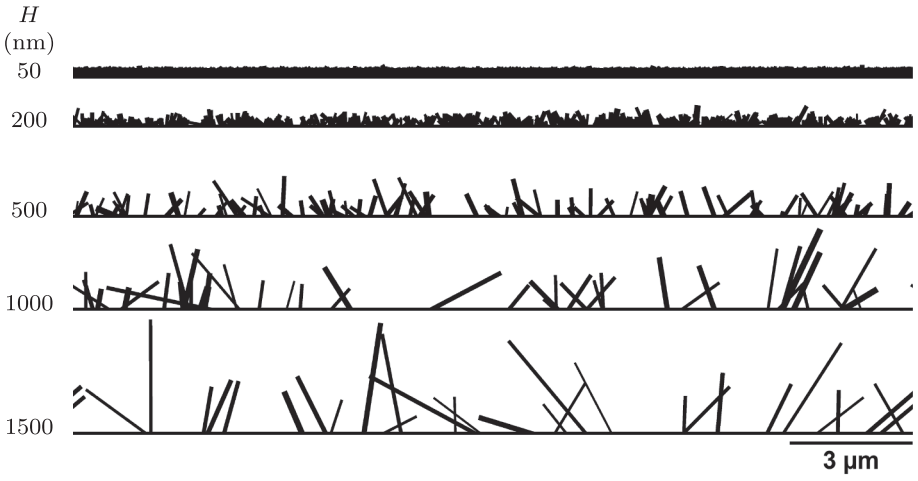

Fig. 2. Like Fig. 1, but with mean filament width 100 nm.

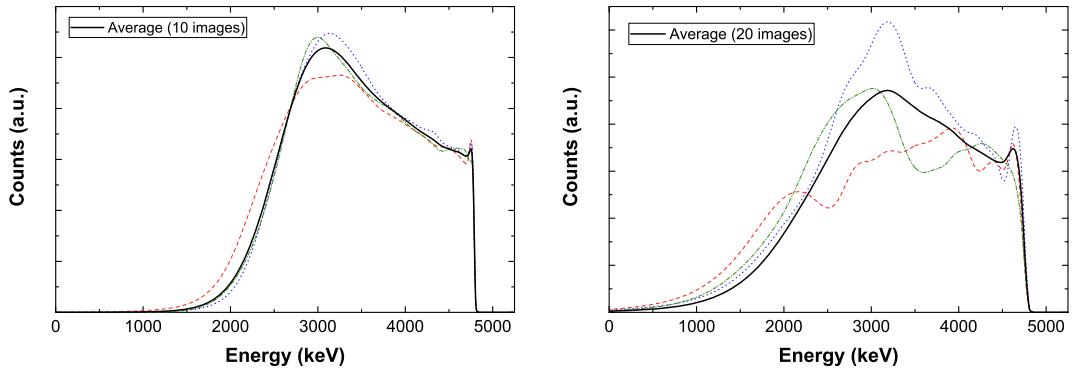

Fig. 3. He recoil spectra for 10 MeV incident ^{16}O ions at a recoil angle of 30° calculated from three different images (dashed red line, dotted blue line, dash-dotted green line) created from the same set of parameters. Left: Mean filament width 25 nm, mean filament height 500 nm, no lower block, see Fig. 1 middle for a typical image (but with lower block). Solid black line: Average spectrum calculated from 10 different images. Right: Mean filament width 100 nm, mean filament height 1500 nm, no lower block, see Fig. 2 bottom for a typical image (but with lower block). Solid black line: Average spectrum for 20 different images. (For interpretation of the references to colour in this figure legend, the reader is referred to the web version of this article.)

to fluctuations of the path length of incident ions inside the material and the increase of the recoil cross-section with decreasing energy: Longer incident path lengths inside material result in an increased energy loss of incident ions and a corresponding increase of the integrated recoil cross-section. Because the samples are thin enough that all recoiling He ions reach the detector, i.e. He recoils do not get stuck in the sample, this results in an increase of He counts when the incident path length distribution gets broader, i.e. for increasing mean filament widths and heights.

The integrated number of He recoils, i.e. the total number of He counts in a spectrum, from image number n is denoted by I_n. All images have a width of 4096 px with 5 nm/px and identical mean filament widths and heights. The BPC is (almost) identical for all images, see Section 2.1. The mean integrated number of He recoils $\bar{I}$ is then simply given by

$$\bar{I} = \frac{1}{N}\sum_{n=1}^{N} I_n,$$

with the square of the standard deviation of the integrated number of He recoils σ_I^2

$$\sigma_I^2 = \frac{1}{N}\sum_{n=1}^{N} (I_n - \bar{I})^2.$$

N is the number of simulated spectra for a given set of parameters. N is listed in Fig. 4 and numerical values for σ_I are tabulated in Table 2. For a filament width of 25 nm σ_I reaches maximum values slightly above 2% for filament heights above 500 nm. These small values are due to the relatively large number of filaments in the 4096 px wide images, see Fig. 1. For a filament width of 100 nm the fluctuations from image to image are larger and σ_I reaches maximum values above 6% for filament heights above 1000 nm. These larger values are due to the smaller number of filaments in the 4096 px wide images, see Fig. 2. Numerical values for σ_I for the case with 75 nm lower block are tabulated in Table 3.

The uncertainty of the mean value $\sigma_{\bar{I}}$ is then given by

$$\sigma_{\bar{I}}^2 = \frac{\sigma_I^2}{N}.$$

The integrated number of He recoils $\bar{I}$ and its uncertainty $\sigma_{\bar{I}}$ are shown in Fig. 5 as deviation from the integrated number of He recoils from a smooth sample. For mean filament heights $\leqslant$ 100 nm the total number of He recoils changes by less than 1% for all investigated filament widths. This only small variation is at least partly due to the presence of the bulk block, see Table 1, which limits statistical fluctuations. For larger filament heights the total number of recoils from fuzz deviates more strongly from the number of recoils from a smooth sample. Nevertheless, the maximum deviation for the number of recoils is still only about 12%. Keeping the very large changes of the material distribution in the fuzzy sample structure in mind, see Figs. 1 and 2, this result is noteworthy and shows, that at least within the investigated range of fuzz parameters the total amount of helium can be determined by ERDA with astonishingly high stability.

Investigation of spectra without lower block yields insight into the influence of the fuzz structure on the shape of spectra. Real fuzz samples require the fuzz to grow starting from a smooth sample, and therefore are expected to have a He-containing layer at the surface of the W bulk. The He content in this layer is not well known, so we assumed the same He concentration as in the fuzz. This sample structure has been simulated by adding a smooth 75 nm thick lower block of W with 1 at% He at the bottom of the fuzz, see Figs. 1 and 2. Simulated He recoil spectra for 10 MeV incident ^{16}O ions are shown in Fig. 6 with the lower block having a thickness of 75 nm for filament widths from 10 to 100 nm and filaments heights up to 1500 nm. Between 6 and 33 spectra from individual images were averaged in order to obtain sufficiently smooth spectra. Due to the additional lower block the spectra extend to lower energies than the spectra without lower block shown in Fig. 4. Qualitatively the influence of the fuzz on the shape of the spectra is similar as in the case without lower block: The low energy edge at about 1500 keV gets broader with increasing filament width and/or height, the high energy edge of the He recoil spectra at around 4800 keV bevels with increasing mean filament widths and/or heights, a surface peak develops with increasing filament width at about 4600 keV, and the shape of the spectra is almost not influenced by the fuzz in the energy range from 2500 to about 4500 keV for the investigated range of filament widths and heights. For a mean filament width of 10 nm all recoiled He ions reach the detector, i.e., there are no particles lost by getting stuck in the sample structure. This changes for mean filament widths of 50 and 100 nm and filament heights above 200 nm: In these cases recoiling He ions can get stuck in the sample structure. This is characterized by a non-vanishing number of counts at zero energy, see Fig. 6 middle and bottom.

The integrated number of He recoils $\bar{I}$ from samples with lower 75 nm thick block and its uncertainty $\sigma_{\bar{I}}$ are shown in Fig. 7 as deviation from the integrated number of He recoils from a smooth sample. For mean filament heights $\leqslant$ 100 nm the total number of He recoils changes by less than 1% for all investigated filament widths. For a filament width of 10 nm and larger filament heights the total number of recoils from fuzz deviates more strongly from the number of recoils from a smooth sample, but the maximum deviation for the number of recoils remains below 4%. This increase is due to the widening of the incident path length distribution and the corresponding increase of the integrated recoil cross-section, as discussed above. For filament widths

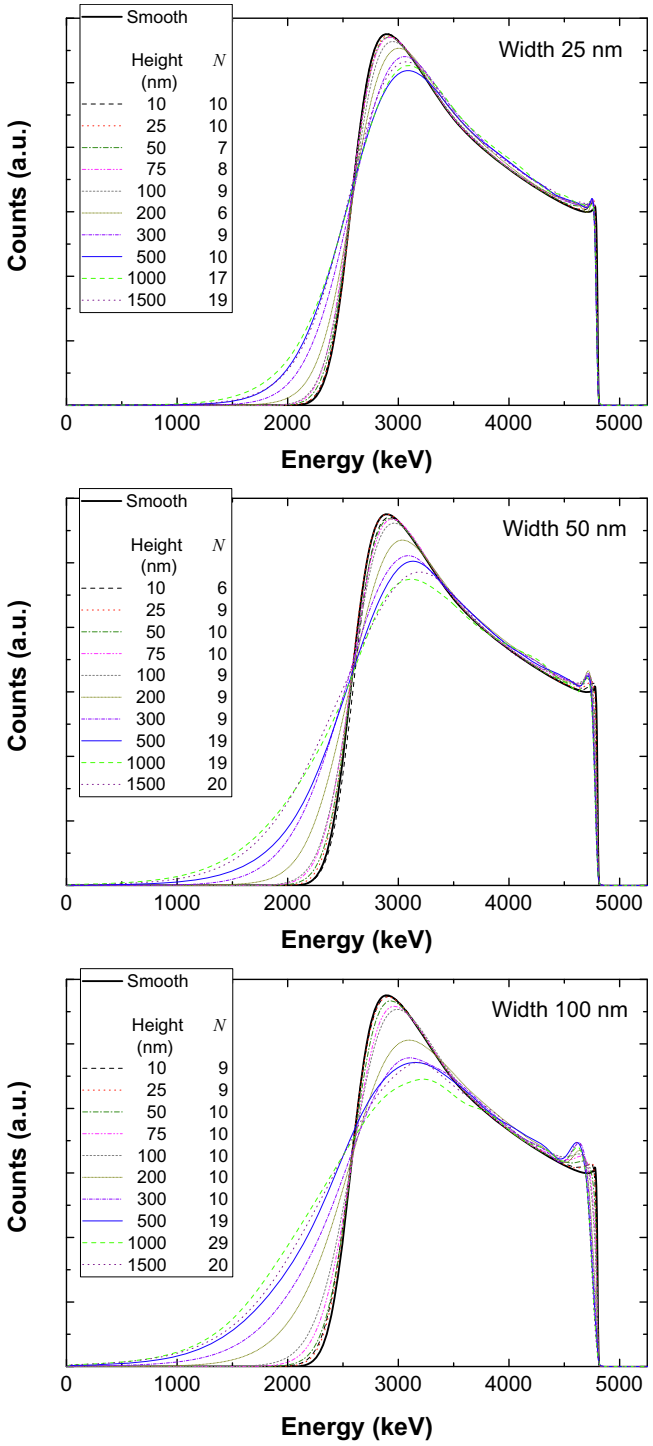

Fig. 4. Averaged He recoil spectra for 10 MeV incident ^{16}O ions at a recoil angle of 30° calculated for different filament widths and heights without lower block. Top: Mean filament width 25 nm; middle: Mean filament width 50 nm; bottom: Mean filament width 100 nm. Typical images of the fuzz structures (with lower block) are shown in Figs. 1 and 2. The number N of averaged spectra is given in the legend.

of 50 and 100 nm one would expect the same increase as already observed for the fuzz samples without lower block, see Fig. 5. This is, however, not observed: For a filament width of 50 nm the integrated number of He recoils stays almost constant (red circles in Fig. 5), for a filament width of 100 nm the integrated number of He recoils even decreases (blue triangles in Fig. 5). This is most probably due to the fact

Table 2
Standard deviation σ_I (in %) of the He count integral for different images with identical mean filament widths W (in nm), heights H (in nm) and number of black pixels. Without lower block, image width 4096 pixels corresponding to 20480 nm.

H	W		
	25	50	100
10	0.18	0.21	0.27
25	0.13	0.15	0.19
50	0.13	0.29	0.30
75	0.38	0.62	0.49
100	0.64	0.66	0.77
200	0.99	0.79	1.05
300	1.80	2.05	1.05
500	2.15	2.21	4.20
1000	2.31	3.11	6.00
1500	2.01	2.85	6.46

Table 3
Standard deviation σ_I (in %) of the He count integral for different images with identical mean filament widths W (in nm), heights H (in nm) and number of black pixels. With lower block having a height of 75 nm, image width 4096 pixels corresponding to 20480 nm.

H	W		
	10	50	100
50	0.10	0.28	0.44
200	0.07	1.19	1.47
500	1.43	1.70	1.64
1000	1.87	3.04	2.94
1500	2.86	3.55	7.18

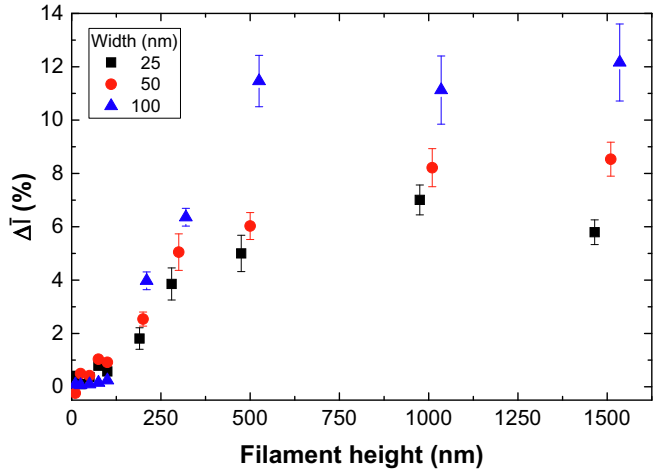

Fig. 5. Deviation of the integrated number of He recoils $\Delta\bar{I}$ from the number of recoils from a smooth sample (in %) for different filament widths as function of filament height. Black squares: Filament width 25 nm; Red circles: Filament width 50 nm; Blue triangles: Filament width 100 nm. For filament heights $\geqslant$ 200 nm the data points are slightly shifted for better visibility. (For interpretation of the references to colour in this figure legend, the reader is referred to the web version of this article.)

that some fraction of the He recoils do not reach the detector, i.e. they get stuck in the sample structure. This effect decreases the total number of detected He recoils and can counterbalance the effect of the increased integrated recoil cross-section. Again, keeping the very large changes of the material distribution in the fuzzy sample structure in mind, see Figs. 1 and 2, this result shows that within the investigated range of fuzz parameters the total amount of helium can be determined by ERDA with astonishingly high stability.

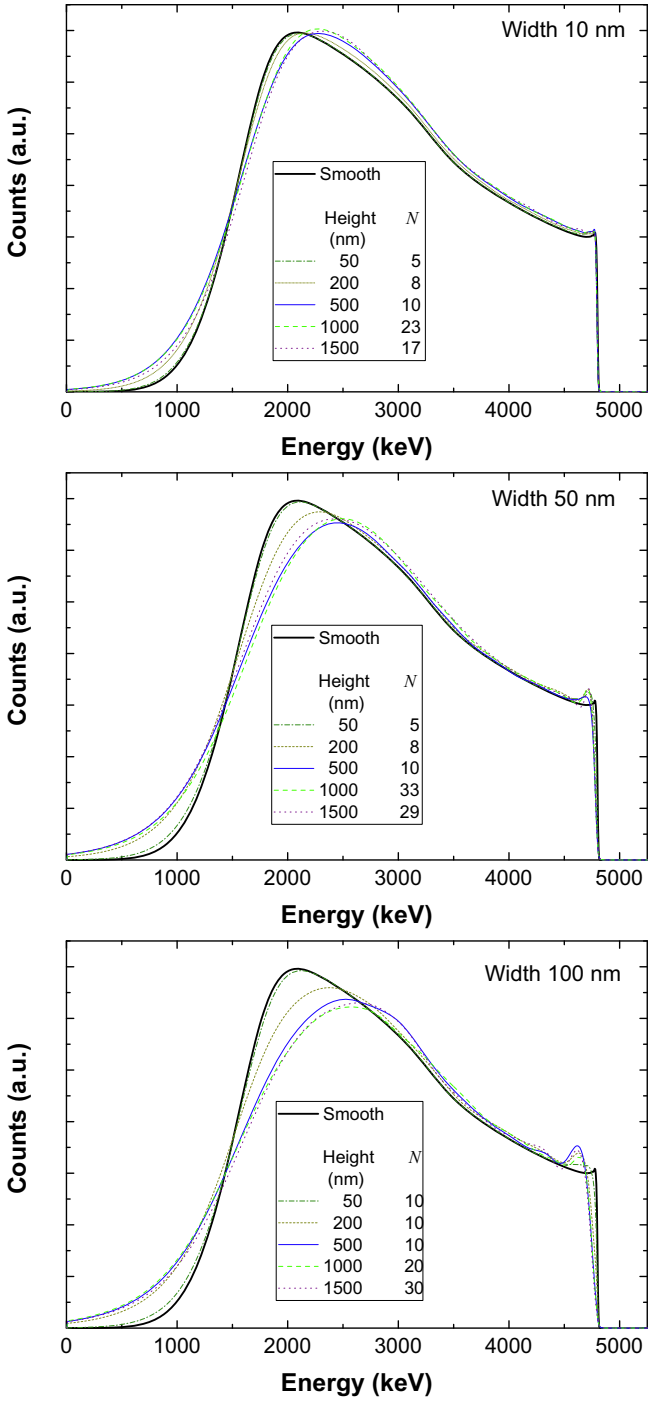

Fig. 6. Averaged He recoil spectra for 10 MeV incident ^{16}O ions at a recoil angle of 30° calculated for different filament widths and heights with 75 nm thick lower block. Top: Filament width 10 ± 5 nm; middle: Filament width 50 ± 15 nm; bottom: Filament width 100 ± 25 nm. Typical images are shown in Figs. 1 and 2. The number N of averaged images is given in the legend.

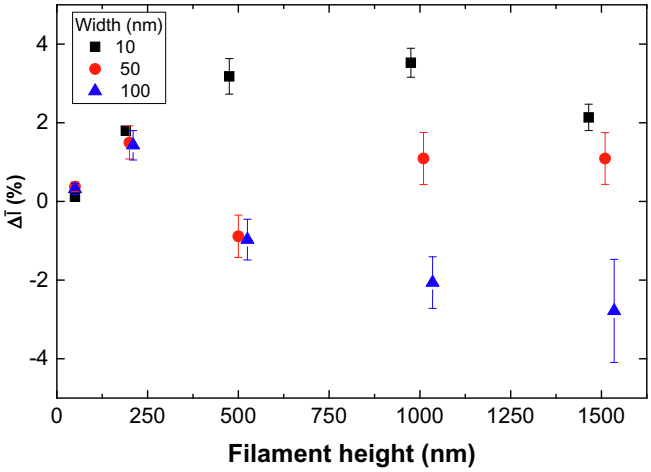

Fig. 7. Deviation of the integrated number of He recoils $\Delta\bar{I}$ from the number of recoils from a smooth sample (in %) for different filament widths as function of filament height. With lower block of 75 nm. Black squares: Filament width 10 nm; Red circles: Filament width 50 nm; Blue triangles: Filament width 100 nm. For filament heights ⩾ 200 nm the data points are slightly shifted for better visibility. (For interpretation of the references to colour in this figure legend, the reader is referred to the web version of this article.)

4. Discussion

Based on the present simplified two-dimensional model of tungsten fuzz the effects of the fuzzy material distribution on energy spectra of He recoils can be summarized as follows:

- The most pronounced effect is a smearing of the low-energy edge of the He energy spectrum. This effect increases with increasing filament width and height and is caused by the widening of the path length distribution inside the material for incident and outgoing ions. This smearing of the low-energy edge has been observed experimentally [[9] Fig. 2], but a more quantitative comparison is difficult due to the lack of quantitative characterization of the fuzz investigated in the experiments.
- Some beveling of the high-energy edge of the recoil energy spectra at larger filament widths. Such a beveling has been observed experimentally [[9] Fig. 2]. However, beveling can be explained also by other effects, especially by a decrease of the He concentration close to the surface.
- The development of a small surface peak due to He recoiling through single filaments. This effect has not been observed experimentally from tungsten fuzz, but a similar effect has been observed experimentally and in computer simulations in Si ERDA spectra from a two-dimensional Si grid structure measured with 200 MeV incident ^{127}I ions [19]. This surface peak therefore may be due to the simplifications in our model, where fuzz filaments are approximated as two-dimensional rectangles with constant width. While a two-dimensional model is probably not too bad for incident and exit particles in the same plane and only minor influence of multiple/plural scattering out from this plane, in a three-dimensional model fuzz filaments would be approximated by cylinders where the path length in the material depends on the entry point into the cylinder.
- Stability of the shape of the higher energy part of recoil energy spectra within a relatively large range of fuzz heights and widths. Shape and height of these parts of spectra from fuzz are almost identical to the spectrum from a smooth sample.
- If all recoiling He ions reach the detector, then the total number of detected He ions increases with increasing fuzz width and height. This is due to the increase of the integrated recoil cross-section with broadening of the incident path length distribution inside the material. However, the fuzzy structure can also lead to recoiling He ions not reaching the detector, i.e. these get stuck in the sample structure. This results in a decrease of the total number of detected He ions. As these two effects counteract each other, the final result depends on the details of the experiment (incident beam energy, detection geometry) and the detailed fuzz structure (filament widths and heights). Nevertheless, within the investigated range of parameters the total number of detected He ions was astonishingly stable and deviated typically only by a few % from the total number of

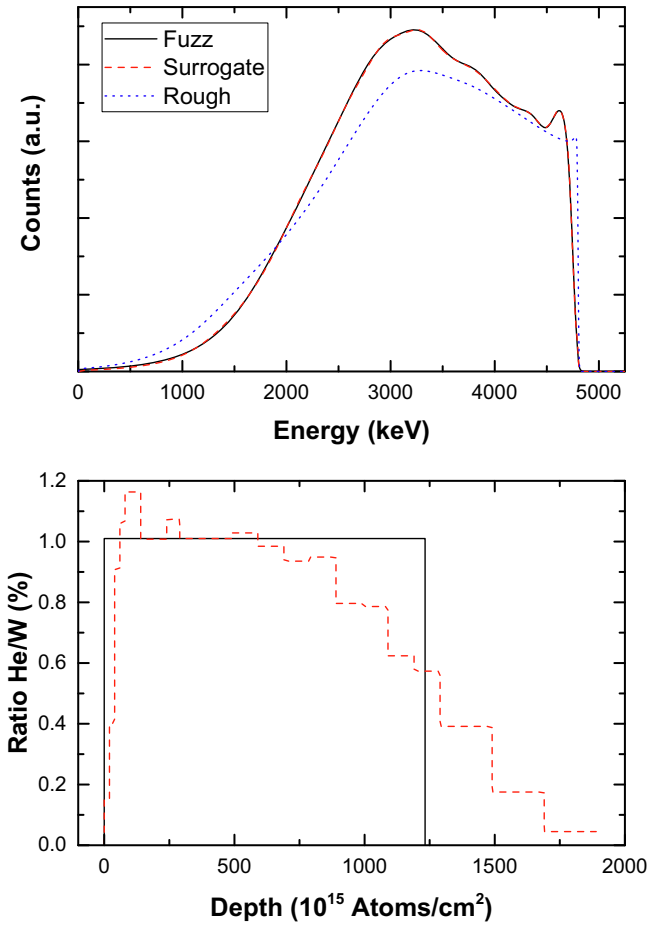

Fig. 8. Top: He recoil spectra for 10 MeV incident ^{16}O ions at a recoil angle of 30°. Solid black line: Calculated from tungsten fuzz without lower block, filament width 100 ± 25 nm, filament height 1000 ± 400 nm, average of 29 spectra (this spectrum is identical to Fig. 4 bottom, dashed green line). Dashed red line: Calculated from a surrogate laterally homogeneous target with layered depth profile. Dotted blue line: Calculated from a rough target based on the incident path length distribution in the material shown in Fig. 9. Bottom: Solid black line: He depth profile in tungsten fuzz; dashed red line: He depth profile in the surrogate target. (For interpretation of the references to colour in this figure legend, the reader is referred to the web version of this article.)

detected He ions from a smooth sample. The maximum observed deviation was about 12%.

Ion beam analysis methods are usually used for depth profiling of elements, i.e. they provide the atomic concentration of elements as function of depth (with the depth scale in atoms/cm^2). The He depth profile for the fuzzy surfaces shown in Figs. 1 and 2 can be obtained by integrating all black pixels in each horizontal row of pixels and then converting the obtained number of atoms to a depth scale in atoms/cm^2. Because all images contain the same number of black pixels and consequently the same number of He and W atoms, the He depth profiles are identical for all fuzzy samples and are shown in Fig. 8 bottom as black line. For a smooth sample without fuzz this He depth profile can be reconstructed from the ERDA spectrum of the He recoils. But for the fuzzy surfaces the question arises: Which information can be extracted from the spectra, and with which accuracy?

A simplified simulation model for backscattering from rough surfaces was developed in [27,28]: The spectrum from a rough layer is constructed as superposition of spectra from smooth surfaces with the statistical weights of the individual spectra based on the frequency distribution of layer thicknesses. Incident and exit particles always

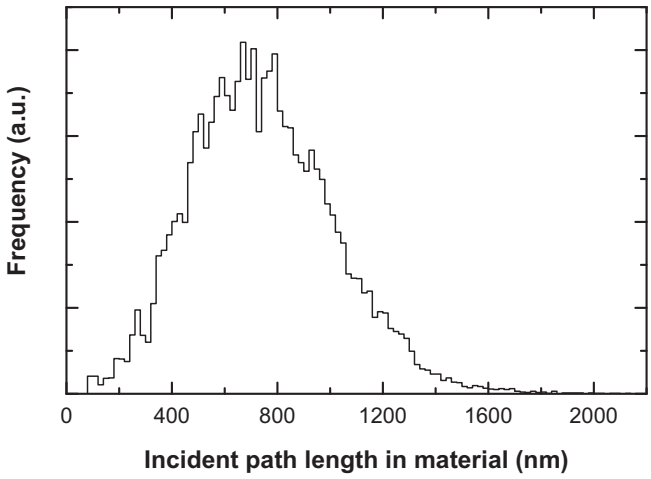

Fig. 9. Path length distribution of incident ions in material for tungsten fuzz without lower block, filament width 100 ± 25 nm, filament height 1000 ± 400 nm, average of 50 images.

traverse the same layer thickness. The path length distribution of incident oxygen ions in material is shown in Fig. 9 for the case of tungsten fuzz without lower block, filament width 100 ± 25 nm, filament height 1000 ± 400 nm. The distribution function is relatively broad with a most probable path length of about 700 nm. The simulated spectrum based on this roughness distribution is shown in Fig. 8 as dotted blue line. While the general shape of this spectrum fits the calculated spectrum from fuzz (black line in Fig. 8), the overall agreement is relatively poor. The high energy edge is too steep because incidence from one side of a fuzz filament and recoiling through the filament cannot be described correctly. This model is therefore too simplified for the case of such extreme roughnesses as tungsten fuzz and the case of ERDA.

The stability of the shape of the higher energy part of the recoil energy spectra together with the relative stability of the total number of detected recoils allows using a surrogate smooth sample with depth profile which gives a recoil energy spectrum identical to the sample with fuzz. This is shown in Fig. 8: The top part shows an average He recoil spectrum calculated from tungsten fuzz without lower block with a mean filament width of 100 nm and a filament height of 1000 nm as solid black line. The dashed red line in Fig. 8 is calculated from a surrogate laterally homogeneous sample with layered depth profile, this depth profile is shown in Fig. 8 bottom. The two spectra are indistinguishable. The He depth profile in the fuzz is constant with a He/W ratio of 1.01 until a depth of 1232.3×10^{15} atoms/cm^2, see Fig. 8 top, the fuzz contains 12.32×10^{15} He-atoms/cm^2. This true depth profile is roughly reproduced by the He depth profile in the surrogate sample. The total amount of He in the surrogate sample is 12.56×10^{15} He-atoms/cm^2, which is a deviation from the correct amount by only 1.9%. The He concentration of 1% is roughly reproduced from the surface up to a depth of about 800×10^{15} atoms/cm^2, and the thickness of the He-containing layer can be roughly estimated. But this example shows also the limitations of the surrogate sample technique: The beveling of the high energy edge is incorrectly attributed to a decay of the He concentration to zero at the surface, the recoil peak close to the surface is incorrectly attributed to a peak in the He concentration, and the smearing of the low-energy edge is incorrectly attributed to a decay of the He concentration. The surrogate sample technique therefore allows deriving only semi-quantitative results for the depth distribution which should be treated with adequate care. The total amount of He can be extracted from the data with considerably higher robustness and accuracy.

A material structure consisting of two randomly distributed phases with different compositions was constructed in [29] and the influence on the shape of RBS spectra was investigated. The results were

qualitatively comparable to the results of the current investigation: Total amounts of elements can be extracted robustly from RBS spectra, while depth profiles obtained from a surrogate sample can be quantitatively inaccurate and have to be treated with care.

Accurate evaluation of ERDA spectra from tungsten fuzz therefore requires taking the correct microstructure of the fuzz into account. A statistical sound evaluation requires very large cross-sectional images with a width of 100 μm or more at high resolution. Typical TEM images of tungsten fuzz, see for example [[7] Fig. 1], are usually much smaller and offer only insufficient statistics of the fuzz structure. This demonstrates the difficulties obtaining statistically sound results for simulations based only on experimental data on the microstructure of tungsten fuzz.

5. Conclusions

The influence of fuzz-like tungsten surface structures on the shape of helium ERDA spectra recoiled by incident 10 MeV ^{16}O ions was investigated by computer simulations using the program STRUCTNRA and a phenomenological tungsten fuzz model. The mean width of the tungsten fuzz filaments was varied from 10 to 100 nm and the mean filament height was varied from 10 to 1500 nm while keeping the total amount of material constant. The He concentration in the fuzz was assumed to be 1 at%.

With increasing fuzz width and height the He ERDA energy spectra show pronounced changes of the spectrum shape: The low-energy edge of the He spectrum smears out, a small surface peak develops, and the high-energy edge of the recoil spectra bevels for larger mean filament widths. The shape of the higher energy part of the recoil spectra stays stable within a relatively large range of mean fuzz heights and widths. For only slowly varying cross-sections (such as the Rutherford cross-section) the total number of recoiling He ions remained surprisingly stable even for very fuzzy surfaces and deviated by less than 12% from a smooth surface within the investigated parameter range.

A surrogate smooth sample with depth profile giving a recoil energy spectrum identical to the sample with fuzz can be always found. The total amount of He can be derived robustly using the surrogate sample with an accuracy better than 2% within the investigated parameter range. However, He depth profiles derived by the surrogate sample technique can be considered only as semi-quantitative and should be treated with some care, as effects caused by the lateral sample microstructure are incorrectly attributed to structures in the concentration depth profiles.

Accurate evaluation of ERDA spectra from tungsten fuzz requires taking the correct microstructure of the fuzz into account. However, even for large images with a width of 4096 pixels (corresponding to image widths of more than 20 μm) the statistical fluctuations from image to image can be large and combined image widths of more than 200 μm were necessary in order to achieve statistically sound results. Since experimental cross-sectional images of samples from SEM or TEM investigations are usually much smaller, this demonstrates the difficulties obtaining statistically sound results based on experimental images of fuzzy sample surfaces.

Acknowledgments

The initial version of the program for generating fuzzy surfaces (see Section 2.1) was developed by K. Kumar, whose work is gratefully acknowledged.

References

[1] S. Takamura, N. Ohno, D. Nishijima, S. Kajita, Formation of nanostructured tungsten with arborescent shape due to helium plasma irradiation, Plasma Fusion Res. 1 (2006) 051.
[2] S. Kajita, S. Takamura, N. Ohno, D. Nishijima, H. Iwakiri, N. Yoshida, Sub-ms laser pulse irradiation on tungsten target damaged by exposure to helium plasma, Nucl. Fusion 47 (2007) 1358.
[3] M.J. Baldwin, R.P. Doerner, Helium induced nanoscopic morphology on tungsten under fusion relevant plasma conditions, Nucl. Fusion 48 (2008) 035001 .
[4] S. Kajita, W. Sakaguchi, N. Ohno, N. Yoshida, T. Saeki, Formation process of tungsten nanostructure by the exposure to helium plasma under fusion relevant plasma conditions, Nucl. Fusion 49 (2009) 095005 .
[5] M.J. Baldwin, R.P. Doerner, Formation of helium induced nanostructure 'fuzz' on various tungsten grades, J. Nucl. Mater. 404 (2010) 165.
[6] R.P. Doerner, M.J. Baldwin, P.C. Stangeby, An equilibrium model for tungsten fuzz in an eroding plasma environment, Nucl. Fusion 51 (2011) 043001 .
[7] Y. Ueda, H. Peng, H. Lee, N. Ohno, S. Kajita, N. Yoshida, R. Doerner, G.D. Temmerman, V. Alimov, G. Wright, Helium effects on tungsten surface morphology and deuterium retention, J. Nucl. Mater. 442 (2013) S267.
[8] K.B. Woller, D.G. Whyte, G.M. Wright, R.P. Doerner, G.D. Temmerman, Helium concentration in tungsten nano-tendril surface morphology using Elastic Recoil Detection, J. Nucl. Mater. 438 (2013) S913.
[9] K.B. Woller, D.G. Whyte, G.M. Wright, Dynamic measurement of the helium concentration of evolving tungsten nanostructures using Elastic Recoil Detection during plasma exposure, J. Nucl. Mater. 463 (2015) 289.
[10] L. Liu, D. Liu, Y. Hong, H. Fan, W. Ni, Q. Yang, Z. Bi, G. Benstetter, S. Li, High-flux He^+ irradiation effects on surface damages of tungsten under ITER relevant conditions, J. Nucl. Mater. 471 (2016) 1.
[11] Y. Gasparyan, V. Efimov, K. Bystrov, Helium concentration measurement in tungsten fuzz-like nanostructures by means of thermal desorption spectroscopy, Nucl. Fusion 56 (2016) 054002 .
[12] M. Bannister, F. Meyer, H. Hijazi, K. Unocic, L. Garrison, C. Parish, Surface morphologies of He-implanted tungsten, Nucl. Instr. Meth. B 382 (2016) 76.
[13] R.P. Doerner, D. Nishijima, S.I. Krasheninnikov, T. Schwarz-Selinger, M. Zach, Motion of W and He atoms during formation of W fuzz, Nucl. Fusion 58 (2018) 066005 .
[14] S. Krasheninnikov, Viscoelastic model of tungsten 'fuzz' growth, Phys. Scr. T145 (2011) 014040 .
[15] Y.V. Martynenko, M.Y. Nagel', Model of fuzz formation on a tungsten surface, Plasma Phys. Rep. 38 (2012) 996.
[16] F. Sefta, K.D. Hammond, N. Juslin, B.D. Wirth, Tungsten surface evolution by helium bubble nucleation, growth and rupture, Nucl. Fusion 53 (2013) 073015 .
[17] A. Lasa, S. Tähtinen, K. Nordlund, Loop punching and bubble rupture causing surface roughening—a model for W fuzz growth, EPL 105 (2014) 25002.
[18] R.P. Doerner, M.J. Baldwin, M. Simmonds, J.H. Yu, L. Buzi, T. Schwarz-Selinger, Quantitatively measuring the influence of helium in plasma-exposed tungsten, Nucl. Mater. Energy 12 (2017) 372.
[19] I. Yesil, W. Assmann, H. Huber, K. Löbner, Simulation of surface roughness effects in ERDA, Nucl. Instr. Meth. B 136–138 (1998) 623, https://doi.org/10.1016/S0168-583X(97)00860-4.
[20] T. Sajavaara, K. Arstila, A. Laakso, J. Keinonen, Effects of surface roughness on results in elastic recoil detection measurements, Nucl. Instr. Meth. B 161–163 (2000) 235.
[21] F. Schiettekatte, M. Chicoine, Spectrum simulation of rough and nanostructured targets from their 2D and 3D image by Monte Carlo methods, Nucl. Instr. Meth. B 371 (2016) 106, https://doi.org/10.1016/j.nimb.2015.09.089.
[22] M. Mayer, Ion beam analysis of rough thin films, Nucl. Instr. Meth. B 194 (2002) 177, https://doi.org/10.1016/S0168-583X(02)00689-4.
[23] M. Mayer, Computer simulation of ion beam analysis of laterally inhomogeneous materials, Nucl. Instr. Meth. B 371 (2016) 90, https://doi.org/10.1016/j.nimb.2015.11.032.
[24] M. Mayer, P. Malinský, F. Schiettekatte, Z. Zolnai, Intercomparison of ion beam analysis software for the simulation of backscattering spectra from two-dimensional structures, Nucl. Instr. Meth. B 385 (2016) 65, https://doi.org/10.1016/j.nimb.2016.08.010.
[25] M. Mayer, SIMNRA User's Guide, Tech. Rep. IPP 9/113, Max-Planck-Institut für Plasmaphysik, Garching, 1997 URL:http://home.mpcdf.mpg.de/mam/Report%20IPP%209-113.pdf.
[26] J. Ziegler, SRIM-2003, Nucl. Instr. Meth. B 219–220 (2004) 1027, https://doi.org/10.1016/j.nimb.2004.01.208.
[27] M. Mayer, J. Roth, K. Ertl, Rutherford backscattering spectroscopy and elastic recoil detection analysis with lithium ions – the better alternative to helium? Nucl. Instr. Meth. B 190 (2002) 405.
[28] H. Langhuth, M. Mayer, S. Lindig, Layer morphology analysis of sputter-eroded silicon gratings using Rutherford backscattering, Nucl. Instr. Meth. B 269 (2011) 1811, https://doi.org/10.1016/j.nimb.2011.05.002.
[29] M. Mayer, T. Silva, Computer simulation of backscattering spectra from paint, Nucl. Instr. Meth. B 406 (2017) 75, https://doi.org/10.1016/j.nimb.2017.01.006.